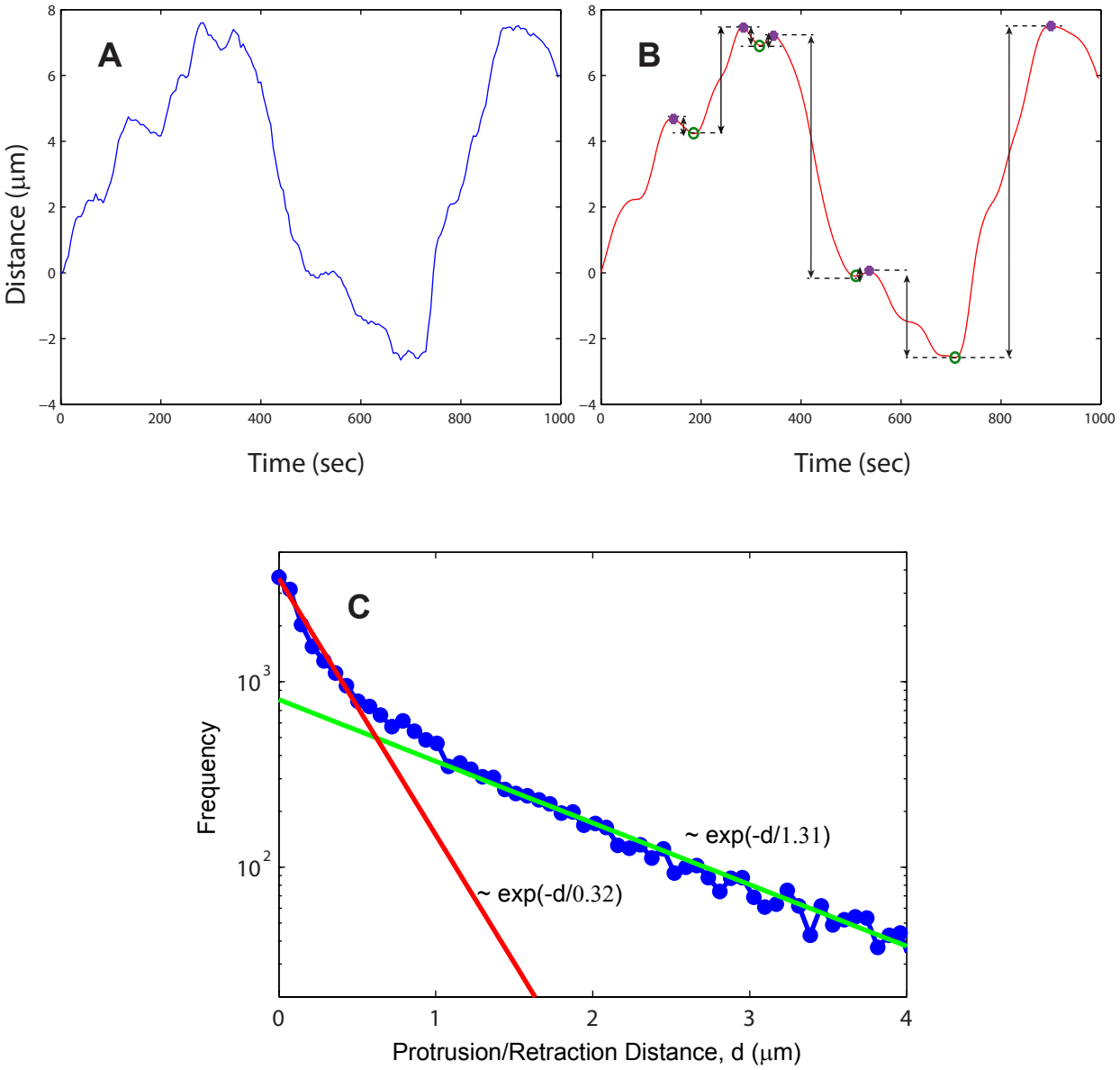

Figure S1. Histogram of protrusion/retraction distances (in relation to Figure 1). (A) Protrusion distance obtained by time-integration of protrusion velocity. (B) Spline-filtered protrusion distance. Arrows indicate protrusion/retraction distances. Open circle (o): protrusion onset, Solid circle (•): retraction onset. (C) The blue line indicates the histogram constructed from n = 2023 protrusion velocity time series in 9 cells pooled from 3 independent experiments. The red line indicates the exponential curve fitted with the data less than 0.72 μm (10 pixel) distance. The green line indicates the exponential curve fitted with the data between 1.4 (20 pixel) and 2.2 μm (30 pixel) distance.

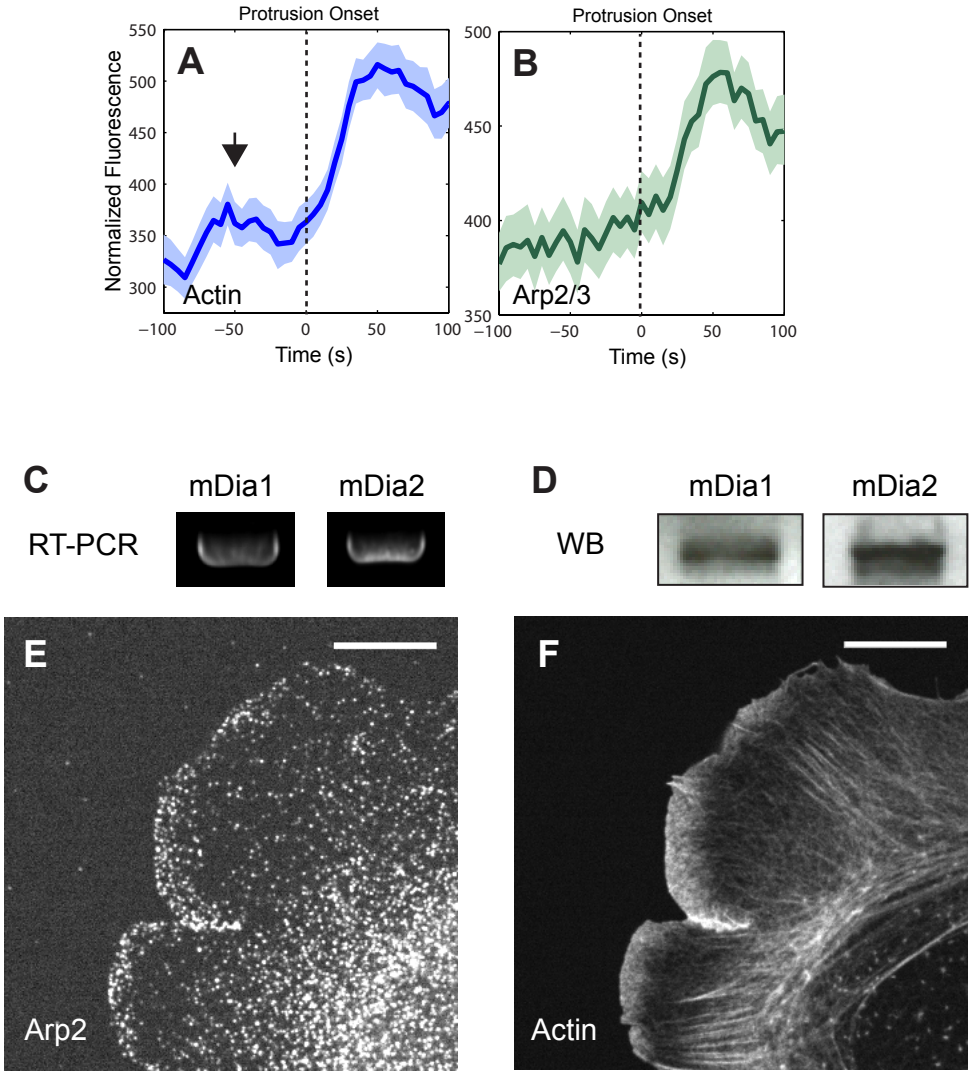

Figure S2. Recruitment of actin before protrusion onset and expression of mDia1 and mDia2 and immune-localization of Arp2/3 in PtK1 cells (in relation to Figure 2). (A-B) Magnified view of Fig. 2B (A) and Fig. 2E (B). The arrow in (A) indicates early recruitment of actin. (C) Reverse-Transcript PCR product confirming the existence of mRNA of mDia1 and mDia2 in PtK1 cells. (D) Western blot confirming the expression of mDia1 and mDia2 in PtK1 cells. (E-F) Immuno-localization of Arp2/3 in a PtK1 cell; (E) Arp2, (F) phalloidin. Scale bars: 10 μm.

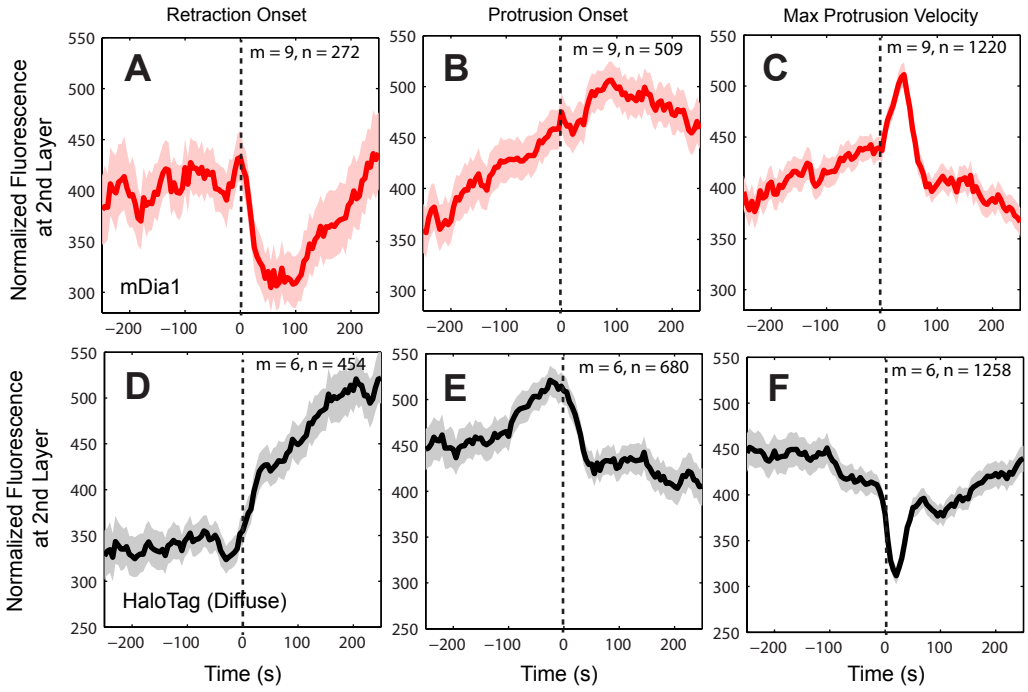

Figure S3. Recruitment of mDia1 to the second layer of probing windows (in relation to Figure 2). mDia1 recruitment underwent a transient dip after maximal protrusion velocity (Figure 2L), suggesting a hand-over from mDia1-based to Arp2/3-based actin nucleation during fast protrusion. To characterize the origin of the dip of mDia1 more closely, we analyzed the fluorescence time series in the second layer of probing windows 0.5 to 1.0 µm from the cell edge. (A-C) Normalized fluorescence intensity time series of HaloTag-TMR labeled mDia1 sampled in the second layer of probing windows (0.5 to 1 µm from leading edge). (D-F) For comparison, diffuse HaloTag-TMR is also sampled in the second layer of windows. Of note, while the recruitment of mDia1 shows marked differences between the first and second window layers (compare time series in (A-C) to those in Fig. 2J-L), the characteristics of the diffuse tag does not change between the two window layers (compare time series in (D-F) to those in Fig. 1K-M). Thus, the sharp decrease in HaloTag-mDia1 fluorescence at the cell edge after maximum velocity is reached is not related to a delay of diffuse TMR label, but to a *bona fide* reduction of HaloTag-TMR labeled mDia1 recruitment to the region of the first window layer. The fact that mDia1 recruitment shows a peak after maximal protrusion velocity (C) suggests that the fast edge movement concurrent with Arp2/3 recruitment displaces mDia1 from the leading edge. For each condition the number *n* of time series sampled in *m* cells pooled from multiple independent experiments (4 for mDia1 and 2 for HaloTag-TMR) is indicated. Solid lines indicate population averages. Shaded error bands about the population averages indicate 95% confidence intervals by bootstrap sampling.

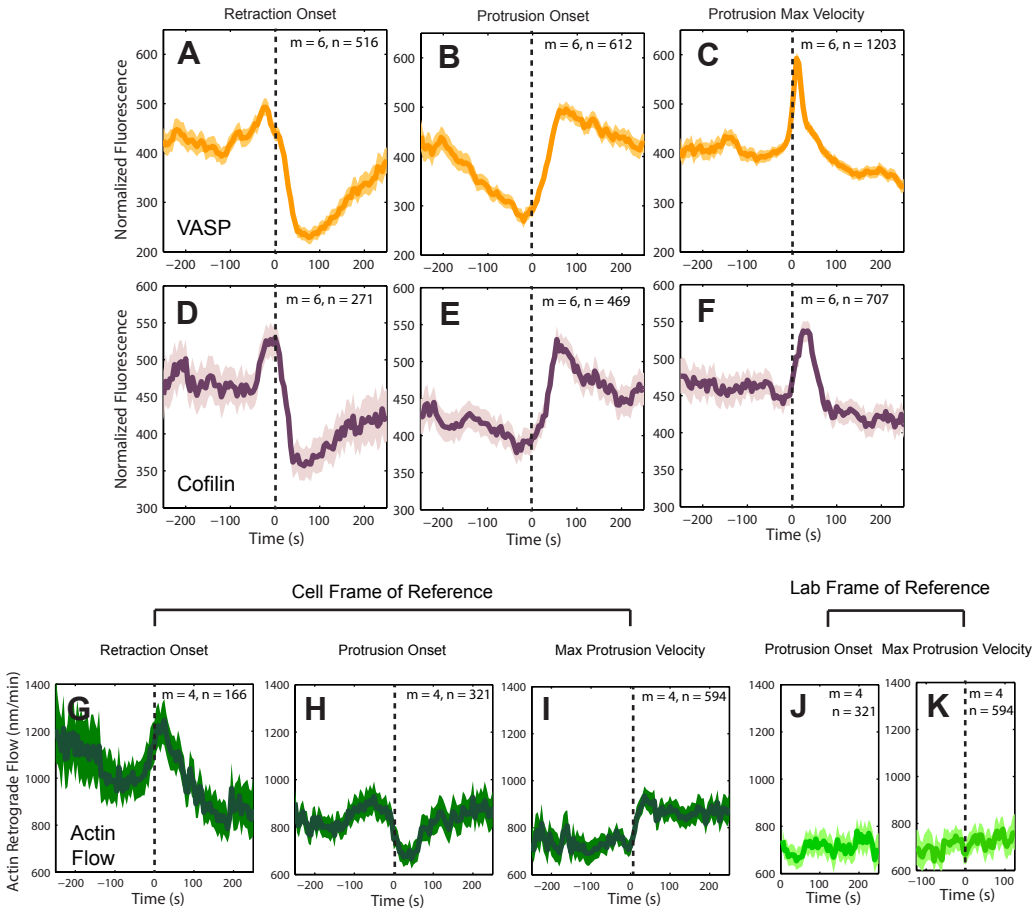

Figure S4. Recruitment of VASP and cofilin to lamellipodium (in relation to Figure 2), and spatiotemporal coordination of actin retrograde flow (in relation to Figure 3). (A-F) Normalized fluorescence intensity time series of VASP and cofilin registered with respect to retraction onset, protrusion onset or maximal protrusion velocity. (G-K) Time series of actin retrograde flow relative to the substrate sampled in cell or laboratory frames of reference registered with respect to retraction onset, protrusion onset or maximal protrusion velocity. The conclusions drawn from our analyses of traction force and adhesion formation are also supported by analysis of actin retrograde flow in the lamellipodia. As nascent adhesions form and mature (Figure 3I-K), actin retrograde flow slows down and remains slow until maximal protrusion velocity is reached in both cell and laboratory frames of reference (G-K). However, as nascent adhesions translocate away from the edge after protrusion onset retrograde flow increases in the cell frame of reference (H-I) but remains stationary in the lab frame of reference (J-K). This offers two additional insights: First, the sharp increase of actin retrograde flow after maximal protrusion velocity (I) indicates that the strongest engagement of actin filaments and adhesions with the substrate occurs before fastest protrusion. Thereafter, a significant portion of the upregulated actin assembly will be converted into filament retrograde flow instead of edge advancement. Second, protrusion initiation is triggered by joint recruitment of components required for the formation of nascent adhesions on the one hand and for actin assembly on the other hand. This yields cooperativity between increased filament growth and decreased filament retrograde flow required for efficient cell edge advancement. For each condition the number *n* of time series sampled in *m* cells pooled from multiple independent experiments (2 for VASP, 3 for cofilin, 3 for actin retrograde flow) is indicated. Solid lines indicate population averages. Shaded error bands indicate 95% confidence intervals computed by bootstrap sampling.

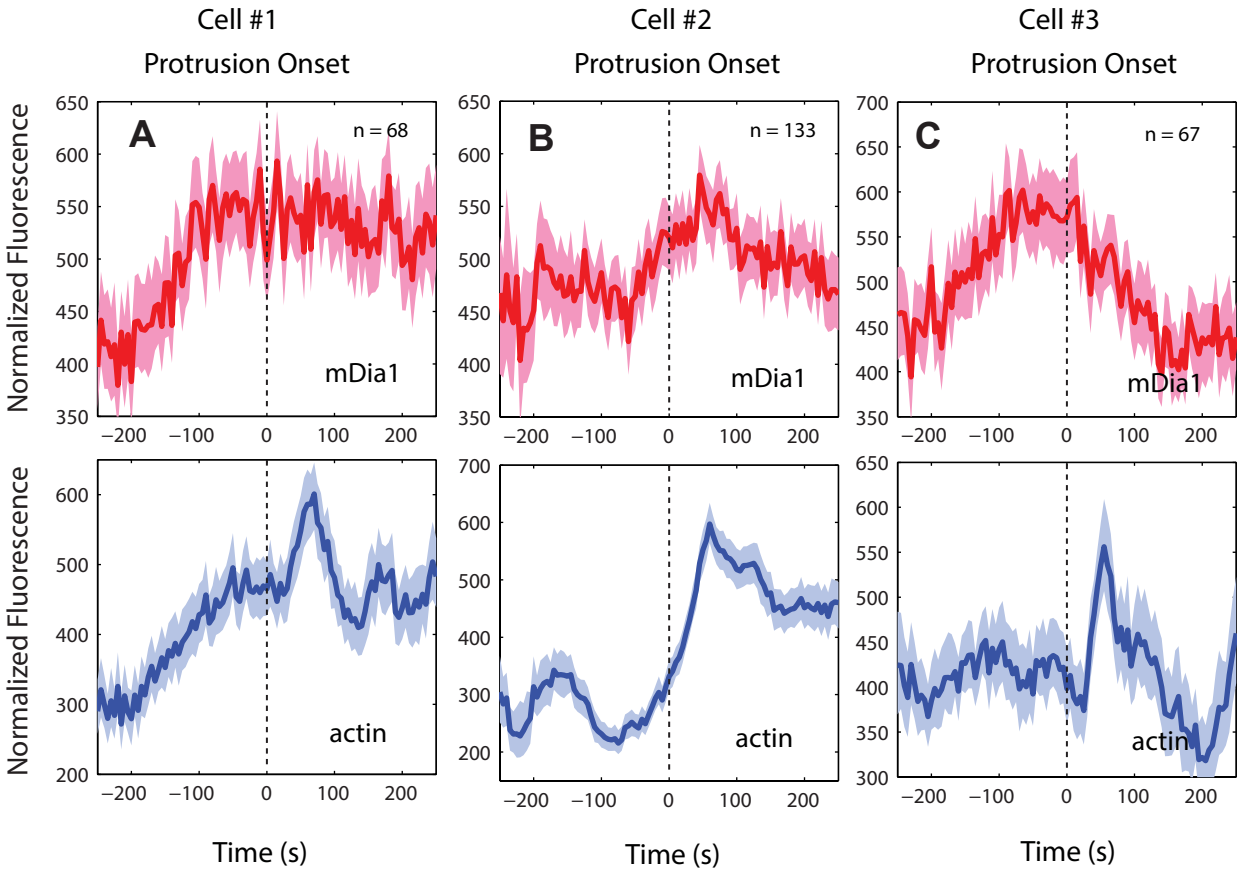

Figure S5. Recruitment of mDia1 and actin to lamellipodium in individual cells (in relation to Figure 4). (A-C) Normalized fluorescence intensity time series registered with respect to protrusion onset. For each cell the number *n* of time series is indicated. Solid lines indicate population averages. Shaded error bands about the population averages indicate 95% confidence intervals by bootstrap sampling.

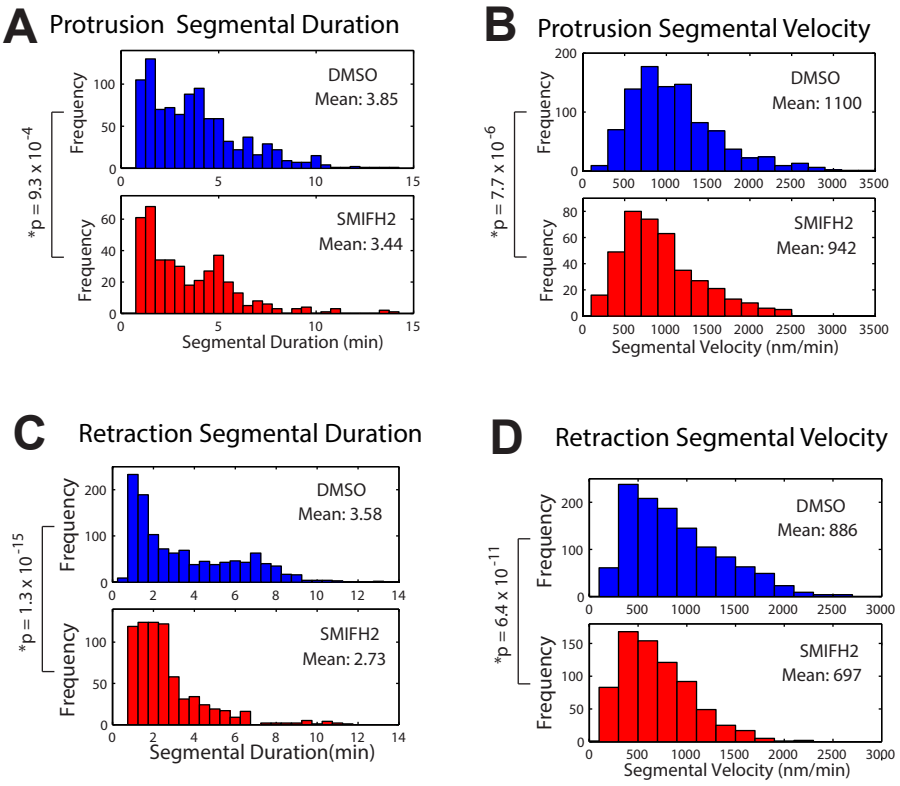

Figure S6. . Effects of formin inhibition on segmental duration and velocity in protrusion and retraction (in relation to Figure 5). (A) Distribution of protrusion segmental duration in DMSO or SMIFH2-treated cells. (B) Distribution of protrusion segmental velocity (average edge velocity in individual protrusion segments) in DMSO or SMIFH2-treated cells. (C) Distribution of duration of retraction segments in DMSO or SMIFH2 treated-cells. (D) Distribution of retraction segmental velocity (average edge velocity in individual retraction segments) in DMSO or SMIFH2 treated-cells. P-values are calculated using two tailed K-S test.

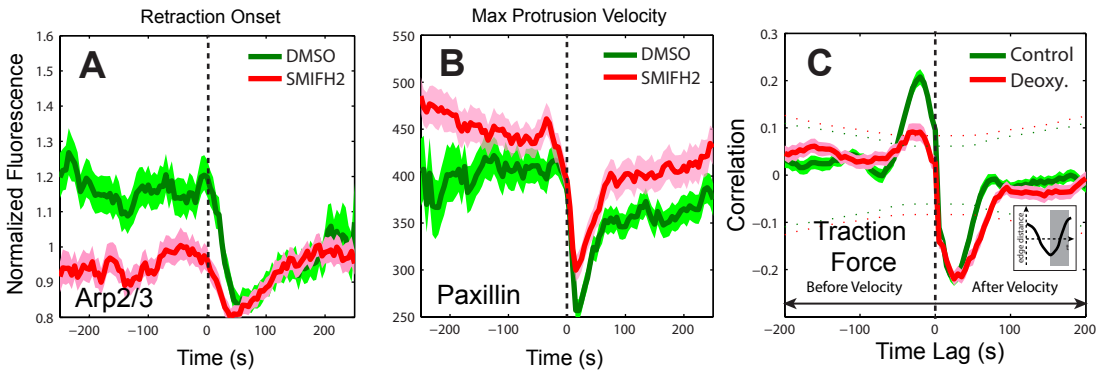

Figure S7. Effects of formin inhibition on Arp2/3 and paxillin at the leading edge (in relation to Figure 5), and effects of membrane tension on correlation between traction force and protrusion velocity (in relation to Figure 6). (A) Time series of Arp2/3 intensity in the lamellipodium normalized to the Arp2/3 intensity in the region 1.5 – 2 μm behind the cell edge are registered with respect to retraction onset in DMSO or SMIFH2-treated cells. n = 321 time series sampled in m = 10 cells for DMSO and n = 391 time series sampled in m = 11 cells for SMIFH2, pooled from 3 independent experiments. (B) Normalized paxillin fluorescence intensity time series in DMSO or SMIFH2-treated cells registered with respect to maximal protrusion velocity. n = 888 time series sampled in m = 8 cells for DMSO and n = 698 time series sampled in m = 11 cells for SMIFH2, pooled from 3 independent experiments. Solid lines indicate population averages. Shaded error bands about the population averages indicate 95% confidence intervals by bootstrap sampling. (C) Pearson's correlation coefficients of traction force in cell frame of reference and edge velocity as a function of time using the time series during protrusion phases in control and deoxycholate (see "Perturbing membrane tension using passive pharmacological methods" in Extended Experimental Procedures) (n = 1020 time series sampled in m = 7 cells for control and n = 552 time series sampled in m = 7 cells for deoxycholate, pooled from 2 independent experiments), Solid lines indicate population averages. Shaded error bands about the population averages indicate 95% confidence intervals computed by bootstrap sampling. Dotted lines (arcs) indicate the significant correlation level with 95% confidence.

Extended Experimental Procedures

Cell culture and imaging conditions. PtK1 cells were cultured in Ham's F12 media (Invitrogen), supplemented with 10% FBS, 0.1 mg/ml streptomycin, 100 U/ml penicillin. They were routinely tested for mycoplasma contamination. Cells were transfected by electroporation using the Neon transfection system (Invitrogen) according to manufacturer's instructions (1 pulse, 1400V, 20ms), and grown on acid-washed glass coverslips from Corning (#1.5 coverslips) for 2 days before imaging. Prior to imaging, expressed HaloTag fusion proteins were labeled by HaloTag-TMR ligand (Promega) according to manufacturer's instructions. For plasma membrane staining in Figure 3 (TFM) and Figure 5, cells were incubated with 1 μg/ml CellMask Orange (Invitrogen) for 5 min, and images were acquired within 2 hours. Imaging was performed in imaging medium (Leibovitz's L-15 without phenol red, Invitrogen) supplemented with 10% FBS, 0.1 mg/ml streptomycin, 100 U/ml penicillin, 0.45% glucose, and Oxyrase (1.0 U per ml , Oxyrase Inc.).

Plasmid construction. Mouse mDia1, mDia2, and VASP were sub-cloned into pFN21A vector (Promega) containing an N-terminal fusion to HaloTag. Human Arp3 and paxillin were subcloned into pFC14K vector (Promega) containing C-terminal fusion of HaloTag according to manufacturer's instructions. pFN21A-cofilin1 was purchased from Promega. For dual color imaging, GFP-mDia1 in C1 vector and SNAP-actin in C1-vector with truncated CMV promoter (kindly provided by Martin Schwartz) were used.

Immunostaining. PtK1 cells grown on acid-washed coverslips for two days were pre-extracted in CB buffer (10mM MES, pH 6.1, 138mM KCl, 3mM $MgCl_2$, 2mM EGTA) with 0.1% Triton-X-100 and 1μg/ml phalloidin for 1 min. Then, the cells were fixed using 1 % glutaraldehyde in CB for 20 min, followed by two washes with 0.4% NaBH4 in PBS for 15 min each. 3 % BSA in PBS was used for blocking. The fixed cells were incubated with primary antibody (1:100

dilution), followed by incubation with fluorescently conjugated secondary antibody (1:200 dilution) (Invitrogen). After extensive washing, actin was stained with Alexa568 or Alexa647-labeled phalloidin (Invitrogen). mDia1 antibody was purchased from Alexis (210-265-R100). mDia2 antibody was kindly provided by Art Alberts (Van Andel Institute, Grand Rapids, MI) or purchased from Abnova (H00081624-A01) . Arp2 antibody was purchased from Santa Cruz Biotechnology (sc-15389).

Light microscopy. All microscopy except paxillin imaging was performed using an inverted Nikon Ti-E microscope (including motorized focus, objective nosepiece, fluorescence filter turret, and condenser turret) with integrated Perfect Focus System with a 60x, 1.4 NA Plan Apochromat objective lens with 1.5x optovar (for traction force microscopy and dual-color imaging, no optovar was used), motorized stage and focus motor from Prior, and custom built 37°C microscope incubator enclosure mounted on a TMC vibration-isolation table. Confocal images were obtained using a Yokogawa CSU-X1 spinning disk confocal head equipped with an internal motorized high speed emission filter wheel and the Borealis modification (Spectral Applied Research) for increased light throughput and illumination homogeneity. Fluorophores were excited by Spectral Applied Research custom laser merge module (LMM-7) equipped with solid state 561 nm (200 mW) and 642 nm (100 mW) lasers. Excitation and emission wavelengths were selected and attenuated with an AOTF and a quad Semrock 405/488/561/647 dichroic mirror, respectively. Alexa-568 was visualized using the 561 laser line and 620/60 emission filter; HaloTag-TMR was visualized using the 561 laser line and 605/70 emission filter (Chroma); for traction force microscopy, far-red fluorescent beads were visualized by the 647 laser line and 700/75 emission filter (Chroma). Images were collected with an ORCA-AG cooled CCD

camera from Hamamatsu and Metamorph software v7.7 (Molecular Devices) without binning. Exposure times were typically 500 ms using 15~30% laser power.

Paxillin recruitment was imaged by total internal reflection fluorescence microscopy using a Nikon Ti-E inverted motorized microscope with integrated Perfect Focus System, Nikon 100x 1.49 NA TIRF DIC objective lens, and Nikon dual-port TIRF/Epi illuminator with motorized laser incident angle adjustment. For lasers, a Spectral Applied Research laser launch was used with 100mW 401nm, 40mW 442nm, 50mW 491nm, 50mW 515nm, 50mW 561nm and 100mW 640nm solid state lasers with a fiber-optic delivery system and AOTF. A Prior Proscan III controller was used for fast excitation and emission filter wheels, fast transmitted and epi-fluorescence light path shutters, and a linear-encoded motorized stage. A Chroma 405/491/561/638 dichroic mirror was used with a 561 laser line and 600/50 emission filter for HaloTag-TMR. In addition to emission filters, a custom Chroma laser notch filter was used in the emission path to further block the illumination light from reaching the camera and to minimize interference patterns. Images were collected with a Hamamatsu ORCA R2 CCD camera and MetaMorph v7.7 (Molecular Devices). Exposure times were typically 500 ms using 30~50% laser power.

Reverse-transcription PCR. PtK1 cells were grown to 50% confluency and total mRNA of PtK1 cells were extracted using RNeasy Kit (Qiagen) according to manufacturer's instruction. cDNA was made from the total mRNA using Sprint RT Complete-Double PrePrimed (Clontech). Five different mammalian (Human, Mouse, Rat, Bovine, *Monodelphis domestica*) mDia1 and mDia2 mRNA sequences were aligned to identify regions of 100% conserved sequence and PCR primers were designed using these regions. The primers for mDia1 are gaaaagcccaattctgctcatag

and tccatggctctgaccag. The primers of mDia2 are gatggaagatatgaatttaaatgaag and tttcaatccacaacgcataaa. After obtaining PCR products, we confirm the results by sequencing.

Western blotting. PtK1 cells were grown to 80% confluency and washed twice with ice-cold PBS. Cells were lysed in RIPA buffer (150 mM NaCl, 1.0% Triton X-100, 0.5% sodium deoxycholate, 0.1% SDS, 50 mM Tris, pH 8.0) containing a protease inhibitor cocktail tablet (Roche), and the adherent cells were scraped off the dish using a cold plastic cell scraper. The cell suspension was transferred to a pre-cooled microcentrifuge tube and incubated at 4°C for 30 min with agitation and spun at 13,000 rpm for 20 min at 4°C to isolate the supernatant. Samples were made by adding 1vol of Laemmli Sample Buffer (Bio-Rad) and were run on SDS-PAGE and then transferred to a PVDF membrane by applying 40 volts for 1 h at 4°C. The membrane was briefly washed in TBS-T (50 mM Tris, 150 mM NaCl, 0.05% Tween-20, pH 7.6) and blocked for 1h at room temperature with 5% milk in TBS-T. It was probed with a 1:1000 dilution of primary antibody (anti-mDia1 from Axxora, anti-mDia2 from Art Alberts) for 1 h, washed, probed with a 1:1000 dilution of the anti-rabbit IgG HRP antibody (Abcam) for 1h, and washed again. The membrane was incubated with SuperSignal West Pico chemiluminescent substrate (Thermo Scientific), and the blot was exposed to film for 10 seconds.

Formin inhibition. PtK1 cells are incubated with 20 μM SMIFH2(Rizvi et al., 2009) (Sigma-Aldrich) for 1 hour. For quantitative comparison of protrusion dynamics, the cells were stained using CellMask Orange as described above after incubation with SMIFH2. Leader cells were imaged within 2 hours after the staining. For HaloTag fusion proteins, HaloTag was labeled with TMR ligands after incubation with SMIFH2.

Traction force microscopy (TFM). Preparation of soft substrates with far-red fluorescent beads for traction force microscopy is described elsewhere(Gutierrez et al., 2011). Briefly, a ~30 μm layer of silicone gel with a refractive index of ~1.49 and Young's modulus of 8 kPa (1:1.4 mixture of parts A and B of QGel 920 by Quantum Silicones; the Young's modulus measured as described elsewhere(Gutierrez et al., 2011)) was created on a #1.5 cover glass at the bottom of a 35-mm culture dish (WillCo-dish®) by spin-coating and curing at 100 ºC for 2 hrs. The surface of the gel was coated with fibronectin and fluorescent tracer particles (40 nm carboxylated far-red fluorescent beads; excitation/emission 690/720 nm, by Invitrogen, Carlsbad, CA) by 15 min room temperature incubation under a solution of 50 μg/ml of fibronectin and 100 μg/ml EDC in PBS, pH 7.4, with the particles added to the solution. The culture dishes were washed 3 times with PBS, and PtK1 cells were seeded at a concentration of $0.3x10^6$ per dish. Prior to imaging, cells were stained with CellMask Orange (Invitrogen) as described above. In order to prevent oxygen exchange to minimize photodamage, the imaging chamber was completely sealed. At the end of a TFM experiment, cells must be lifted off the substrates in order to measure the position of the tracer beads when the substrate is not deformed by cellular forces. To accomplish this in a closed chamber, the dish covers were outfitted with inlet and outlet tubing and sealed against the dishes with VALAP, making it possible to inject trypsin into the dish. Images of cells and tracer particles were taken (in two different fluorescence wavebands) every 5 seconds for ~1000 seconds on the Nikon Ti spinning disk confocal microscope with a 60x/1.4 objective. Cells were then removed from the substrate by 1 hr incubation in Trypsin/EDTA (10x, 0.5%, Invitrogen), and images of tracer particles on the deformation-free gel substrate were acquired in the areas where cells and particles were imaged beforehand. Cell traction forces were calculated by

comparing images of tracer particles with and without cells on the substrate using the Fourier transform traction cytometry method(Butler et al., 2002).

Perturbing membrane tension using passive pharmacological methods Two approaches have been established to manipulate membrane tension: active methods, which apply pulling force on the membrane (Houk et al., 2012; Raucher and Sheetz, 2000) and passive pharmacological methods (Gauthier et al., 2011; Raucher and Sheetz, 2000; Sedzinski et al., 2011), which alter the structure of the membrane. Both techniques result in equilibration of tension state over short time scales (Houk et al., 2012). To enable high resolution imaging in a closed chamber while manipulating tension level, we chose to perturb tension homeostasis by established passive methods that apply 400 μM deoxycholate (Raucher and Sheetz, 2000) or 1 μg/ml concanavalin A (Con A) (Sedzinski et al., 2011) to globally reduce or increase membrane tension. We validate the effect of perturbing membrane tension on the overall force levels by traction force measurements after deoxycholate treatment. In order to verify the mechanical effects of the passive methods used in our experiments to perturb membrane tension homeostasis, we performed traction force measurement with deoxycholate treatment. Analysis of traction force dynamics in the cell frame of reference in control or low membrane tension (deoxycholate treatment) revealed that the positive correlation peak between edge velocity and traction force is sensitive to membrane tension (Figure S7C). The disappearance of the positive correlation under deoxycholate treatment means that there is no mechanical load on the growing actin filaments during protrusion in low membrane tension, which confirms the validity of our experiments. Since in the cell frame of reference the force-bearing adhesion zone is translocated away from the advancing edge, we also observed the negative correlation dip between edge velocity and traction force (Figure S7C).

Perturbation of tension homeostasis. To manipulate membrane tension, PtK1 cells transfected with Arp3-HaloTag , HaloTag-mDia1, or GFP-Rac1 are incubated with either 400 μM deoxycholate (Sigma-Aldrich) for 30 minutes (decreasing membrane tension) or 1 μg/ml concanavalin A (Invitrogen) for 10 minutes (increasing membrane tension) and washed by media before imaging. For HaloTag fusion proteins, HaloTag was labeled with TMR ligands before incubation with deoxycholate or concanavalin A.

Quantitative fluorescence speckle microscopy. Microinjection of Alexa 561 labeled actin (Invitrogen) into PtK1 cells and quantitative fluorescence speckle microscopy are described elsewhere(Danuser and Waterman-Storer, 2006; Lim and Danuser, 2009). Details of the procedures for actin flow analysis are explained elsewhere(Mendoza et al., 2012).

Cell edge tracking and windowing. Rates of protrusion and retraction were obtained from fluorescence images by computational edge tracking using a custom-built software package written in Matlab (Mathworks). Cell edges were segmented by intensity thresholding and cell edge displacements were tracked by applying the mechanical model described elsewhere(Machacek and Danuser, 2006) for morphing the edge between consecutive time points. Probing windows were generated with a window size of 500 nm by 500 nm for fluorescence intensity analysis and 1 μm by 1 μm for traction force analysis, respectively. The number of windows along the open cell boundary were held constant. Therefore, as the length of the boundary changed, the window size changed as well. The corners of the windows followed the cell edge displacement vectors. The basic concepts of sampling image signals in motile cells have been introduced elsewhere (Machacek et al., 2009). The specifics and validation of a new version of window-based sampling applied for the present study are detailed elsewhere (Elliott, 2015).

Identification of protrusion/retraction segments. Our statistical framework requires robust detection of the onsets of protrusion and retraction for event alignment. Due to intrinsic variations in the protrusion-activating molecular processes as well as measurement noise, protrusion and retraction events proper are stochastic and they are superimposed by random fluctuations. We designed an algorithm to identify among the measured edge movements significant protrusion and retraction events on a per-window basis:

To eliminate small, noisy motion fluctuations, the instantaneous edge velocity measured for a particular window was integrated over time, resulting in an edge displacement time series (Figure S1A). The time series then was filtered by a smoothing spline filter using the Matlab function *csaps*() and a smoothing parameter of 0.01 (Figure S1B). Even though this filtering operation removed noisy motions, the displacement distance time series still contained small protrusion and retraction events that are insignificant in terms of the overall cell edge morphodynamics, as illustrated in Figure S1B. To eliminate those from the pool of protrusion and retraction events eventually used for event alignment and analysis of underlying molecular activities, we next identified local maxima/minima in the edge displacement time series using the Matlab function *findpeaks*(); and derived from them the net protrusion/retraction distances for each event (arrows in Figure S1B). The distribution of distances (Figure S1C) can be decomposed into two exponential distributions, one with a length scale of 0.32 μm and one with a length scale of 1.31 μm (red and green curves in Figure S1C). We focused our analysis on persistent events with distances larger than 0.72 μm (10 pixel length). Less persistent events were excluded from the present analysis. A distance of 10 pixels corresponds to ~1.5 the depth of the probing windows, i.e. only protrusion segments that yielded a significant translocation of the region of interest used for fluorescence intensity sampling were considered.

In addition, we eliminated short-term switches between protrusion and retraction phases by retaining only the highest of the local maxima in a rolling window of 50 seconds. Between every pair of consecutive local maxima we then identified the lowest local minimum, bisecting the interval between the two maxima into a retraction segment lasting from the first local maximum to the local minimum and a protrusion segment lasting from the local minimum to the second local maximum. Protrusion and retraction segments with a distance between endpoints of less than 10 pixels (equals to 720 nm) were again discarded as explained above.

For the retain protrusion/retraction segments, we then computed the segmental distance, the segmental duration, and the average segmental protrusion/retraction velocity (Figure 5D). Distributions of segmental parameters between different experimental conditions were statistically compared using the two-sample KS (Kolmogorov-Smirnov) test (Matlab function *kstest2*()).

Event alignment of intensity time-series and averaging. Time-series of fluorescence intensities in individual windows were aligned relative to protrusion or retraction onsets by copying the sequence of intensity samples prior to the onset into the negative-indexed columns of a space-time matrix, the intensity sample at the onset into column with index zero, and the sequence of intensity sample posterior to the onset into the positive-indexed columns (Figure 1E-F). Sequences prior to the protrusion/retraction onset were limited by the preceding retraction/protrusion onset; and sequences posterior to protrusion/retraction onset were limited by the subsequent retraction/protrusion onset. Average intensity time series, which represent the average kinetics of recruitment of particular fluorescently-tagged fusion proteins, were then computed as the per-column averages of the thus assembled space-time matrices. The 95% confidence intervals about the average series were obtained by bootstrap resampling (Matlab

function *bootci*()). Note that the further away a matrix column is from the central zero-indexed column the fewer intensity samples it contains, weakening the statistics. Thus, predictions about the protein recruitment are most accurate for the few time points before and after the event used for alignment.

To align intensity time-series with respect to maximal protrusion velocity, the time point of maximal velocity was identified in each protrusion segment by fitting a smoothing spline to the corresponding sequence of edge protrusion velocities (using a smoothing parameter of 0.1) and a search for the highest local maximum in the spline. The event alignment of the fluorescence intensity series was then accomplished in the same way as described before for alignments with respect to protrusion/retraction onsets.

Sampling of paxillin fluorescence associated with nascent adhesions. To track the recruitment of fluorescently-tagged paxillin to nascent adhesions it was necessary to filter out the image contributions from focal adhesions. Focal adhesions were segmented by first subtracting local image background, which was estimated by applying a Gaussian low-pass filter with a full-width half-maximum of 10 pixels (corresponding to 630 nm). Using this setting, nascent adhesions disappear in the background. Local-background subtracted images were then binarized into foreground (adhesion) and background (everything else) by applying a global threshold. The threshold level was calculated by combining the Otsu(Otsu, 1979) and Rosin methods(Rosin, 2001) according to $1/3\,\mathrm{OtsuLevel} + 2/3\,\mathrm{RosinLevel}$. Objects with an area greater than 100 pixels (corresponding to 0.4 μm^2) were considered to be focal adhesions. Despite the general suppression of nascent adhesions during background subtraction, aggregates of nascent adhesions at the leading edge occasionally passed the binarization. To further distinguish those aggregates from *bona fide* focal adhesions, we used the criterion that focal adhesions tend to

align perpendicular to cell edges and undergo slow turn-over whereas aggregates of nascent adhesions are parallel to the cell edge and undergo fast turn-over. Algorithmically, we detected *bona fide* focal adhesions by assembling a binary space-time matrix in which probing windows that overlap at a particular time point with the foreground pixels of the segmented paxillin-intensity image are labeled 1 and 0 otherwise. In this data representation long-lived adhesion structures aligned perpendicular to the cell edge generate horizontal streaks, whereas short-lived structures along the cell edge generate vertical streaks. Accordingly, we eliminated all windows from the analysis of paxillin recruitment that belonged to a region in the space-time matrix larger than 10 units and whose primary axis of extension was +/- 20 degrees parallel to the horizontal (time) axis.

Normalization of fluorescence signals in Figures 1K-M, 2, 3I-M, 5L, 6G-H, S3, S4A-F, S5, S7B. Due to the difference in expression level of fluorescent proteins, registered time series of fluorescence intensity could not be averaged at an absolute intensity level. Moreover, each protrusion and retraction event even within the same cell can start at a different base level of protein concentration. Our goal here was to determine the recruitment characteristics for a particular actin modulator or paxillin independent of the baseline. Therefore, we normalized the intensity time series of each window separately, before protrusion event registration and averaging of intensities within one cell and between cells. The normalized fluorescence intensity series for a particular window was calculated as $I_{\mathrm{norm}}(w,t) = (I(w,t) - \min(I(w,t)))/(\max\big(I(w,t)\big) - \min(I(w,t))) \times 1000$.

Normalization of fluorescence signals in Figure 5I-K, 6C-D, S7A. To compare Arp2/3 levels in cells without and with treatment by formin inhibitor, the fluorescence in the lamellipodia had to be normalized relative to the fluorescence in the lamella region. Average background

fluorescence outside cells was subtracted from the fluorescence signal inside the cell. Subsequently, the average intensity of the probing window bands between 1.5 μm and 2 μm from the cell edge was determined as the reference value. The normalized intensity in the lamellipodium was computed as the average value in the band 0.5 μm to 1 μm from cell edge (the second layer of windows) divided by this reference value. To compensate for global intensity fluctuations, e.g. associated with minor focus drift, the normalization was done in each time frame independently, i.e. the division by reference intensity was applied before event registration and averaging of time series.

Correlation analysis of two time series data as a function of time lag. Pearson's correlation coefficient between two time series as a function of time lag is described elsewhere(Machacek et al., 2009). For the correlation analysis between traction force and edge velocity (Figure 3N-P), the time series were divided after identification of protrusion/retraction segments into retraction, early protrusion (from protrusion onset to 50 second before maximal protrusion velocity) and late protrusion (from protrusion onset to 50 second after maximal protrusion velocity) sub-segments. The correlation analyses were performed separately in each time series sub-segment. For the correlation analysis between traction force and edge velocity (Figure S7C), the correlation analyses were performed using time series of protrusion segments (from protrusion onset to 75 second after maximal protrusion velocity) only. The 95% confidence intervals about the average correlation were obtained by bootstrap resampling (Matlab function *bootci*()). The significant correlation level with 95% confidence was calculated by $1.96/\sqrt{N}$, where N is the number of samples.

Correlation analysis of two molecular processes. For the pairwise correlation analysis of mDia1 and actin in Figure 4A-C, we used dual-color time-lapse movies of EGFP-mDia1 vs

SANP-tag-TMR-actin. We sampled the fluorescence signal in the region 0.5 - 1 μm behind the edge in order to avoid noise contamination from the edge boundary. In order to combine the data from multiple cells, each sampled fluorescence map in each cell was first normalized to have the mean of 0 and the standard deviation of 1. The normalized time series were registered with respect to protrusion onset at t = 0, and we calculated Pearson's correlation coefficient (Matlab function *corrcoef*()) between mDia1 at t_1 and actin at t_2, where t_1 and t_2 are measured relative to the protrusion onset.

For the correlation analysis in Figure 4D-F we used the dual-color time-lapse movies of EGFP-mDia1 vs SNAP-tag-TMR-actin, and EGFP-mDia1 vs Arp3-HaloTag-TMR. Again, we sampled the fluorescence signal in the region 0.5 - 1 μm behind the edge and registered the time series with respect to protrusion onset at t = 0. The mean retraction fluorescence signal of mDia1 and actin in each probing window was obtained by averaging the time series with $t < 0$. The mean protrusion fluorescence signal of actin and Arp2/3 in each probing window was obtained by averaging the time series with $t > 0$. To combine data from multiple cells, each mean retraction/protrusion fluorescence signal in each cell was first normalized to 0-mean and standard deviation 1. Then, Pearson's correlation coefficients were calculated (Matlab function *corrcoef*()). To characterize the correlation baseline for unassociated data, we performed the same correlation analysis with randomized data. We did not find any significant correlation with the randomized data.

Correlation analysis of neighboring probing windows registered to protrusion events. In order to test statistical independence of time series used to compute the average recruitment dynamics of proteins, we performed cross correlation analysis between protrusion velocity time series measured in different neighboring probing windows. For initial noise filtering, the edge

velocity measured for a particular window was integrated over time, resulting in an edge displacement time series, followed by a smoothing spline filter using the Matlab function *csaps*() and a smoothing parameter 0.01. The smoothed displacement time series was differentiated to produce the filtered edge velocity time series. Edge velocity time series were registered with respect to retraction onsets, protrusion onsets, and maximal protrusion velocities. Next, we found all pairings between probing windows at particular window distance and cross-correlated corresponding velocity time series pairings between -50 s to 50 s (11 time frames) about the reference events. The correlation functions were averaged over all pairings and over multiple cells. The 95% confidence intervals about the average correlation were obtained by bootstrap resampling (Matlab function *bootci*()). The significant correlation level with 95% confidence was calculated by $1.96/\sqrt{N}$, where *N* is the number of samples.

General Statistical Methods. Sample size: we generally use more than 100 probing windows from multiple cells (see individual figures or figure legends). The sample size is deemed sufficient when the averaged time series displays a distinct pattern with variations that substantially exceed the 95% confidence interval.

Inclusion/exclusion of samples: we visually examined the morphology, the level of protein expression, and the number of nuclei in each cell movie. We performed our analysis in cells with a flat, minimally ruffling morphology and wide leading edges, low expression level of fluorescent proteins, and single nucleus. At this stage, the investigator did not know how the protein dynamics would behave and thus this data selection can be assumed unbiased for the purposes of the presented analyses.

Justification of statistical tests: we used two-sample K-S (Kolmogorov-Smirnov) test for statistical tests. The K-S test makes no assumption about the distribution of data. The variances of the data between groups are similar (See each figure).

Supplemental Movie Legends

Data File1:Movie S1. Heterogeneity and transience of protrusion velocity. Protrusion (green to red colors) and retraction (green to blue colors) velocities tracked in 500 nm-long edge sectors (explained in Figure 1B). Scale bar: 10 μm. Original movie captured at a 5s frame interval; replay at 30 frames/second.

Data File1:Movie S2. Heterogeneity and transience of protrusion/retraciton duration Normalized times since protrusion (green to red colors)/retraction (green to blue colors) onset for each of the sectors tracked in (Movie S1) (explained in Figure 1C). Scale bars: 10 μm. Original movie captured by spinning disc confocal microscopy at a 5s frame interval; replay at 30 frames/second.

Data File1:Movie S3. Probing windows. Overlay of two layers of sampling windows (500 nm x 500 nm) on the raw image data of Movie S5. Scale bar: 5 μm. Replay at 30 frames/second.

Data File1:Movie S4. Fluorescence intensity of HaloTag-TMR in a PtK1 cell. Scale bar: 5 μm. Original movie captured by spinning disc confocal microscopy at a 5s frame interval; replay at 30 frames/second.

Data File1:Movie S5. Fluorescence intensity of microinjected Alexa 568-actin in a PtK1 cell. Scale bar: 5 μm. Original movie captured by spinning disc confocal microscopy at a 5s frame interval; replay at 30 frames/second.

Data File1:Movie S6. Fluorescence intensity of Arp3-HaloTag-TMR in a PtK1 cell. Scale bar: 5 μm. Original movie captured by spinning disc confocal microscopy at a 5s frame interval; replay at 30 frames/second.

Data File1:Movie S7. Fluorescence intensity of HaloTag-TMR-mDia1 in a PtK1 cell. Scale bar: 5 μm. Original movie captured by spinning disc confocal microscopy at a 5s frame interval; replay at 30 frames/second.

Data File1:Movie S8. Fluorescence intensity of HaloTag-TMR-mDia2 in a PtK1 cell. Scale bar: 5 μm. Original movie captured by spinning disc confocal microscopy at a 5s frame interval; replay at 30 frames/second.

Data File1:Movie S9. Fluorescence intensity of HaloTag-TMR-VASP in a PtK1 cell. Scale bar: 5 μm. Original movie captured by spinning disc confocal microscopy at a 5s frame interval; replay at 30 frames/second.

Data File1:Movie S10. Fluorescence intensity of HaloTag-TMR-cofilin in a PtK1 cell. Scale bar: 5 μm. Original movie captured by spinning disc confocal microscopy at a 5s frame interval; replay at 30 frames/second.

Data File1:Movie S11. Traction forces (blue to red colors) in a PtK1 cell. Yellow line: cell edge. Scale bar: 10 μm. Original movie captured by spinning disc confocal microscopy at a 5s frame interval; replay at 30 frames/second.

Data File1:Movie S12. Fluorescence intensity of paxillin-HaloTag-TMR in a PtK1 cell. Scale bar: 5 μm. Original movie captured by total internal reflection microscopy at a 5s frame interval; replay at 30 frames/second.

Data File1:Movie S13. Sampling windows in laboratory/cell frames of reference. Overlay of sampling windows in the laboratory (red) and cell (yellow) frames of reference on the raw image data of Movie S12. Scale bar: 5 μm. Replay at 30 frames/second.

Supplemental References

Butler, J.P., Tolic-Norrelykke, I.M., Fabry, B., and Fredberg, J.J. (2002). Traction fields, moments, and strain energy that cells exert on their surroundings. Am. J. Physiol. Cell Physiol. *282*, C595-605.

Danuser, G., and Waterman-Storer, C.M. (2006). Quantitative fluorescent speckle microscopy of cytoskeleton dynamics. Annu. Rev. Biophys. Biomol. Struct. *35*, 361-387.

Elliott, H., S. Chen, K. Lee, M. Mendoza, S. Besson, G. Danuser (2015). Quantification of image patterns in dynamics and variable cell shapes. Submitted.

Gauthier, N.C., Fardin, M.A., Roca-Cusachs, P., and Sheetz, M.P. (2011). Temporary increase in plasma membrane tension coordinates the activation of exocytosis and contraction during cell spreading. Proc. Natl. Acad. Sci. USA *108*, 14467-14472.

Gutierrez, E., Tkachenko, E., Besser, A., Sundd, P., Ley, K., Danuser, G., Ginsberg, M.H., and Groisman, A. (2011). High refractive index silicone gels for simultaneous total internal reflection fluorescence and traction force microscopy of adherent cells. PLoS One *6*, e23807.

Houk, A.R., Jilkine, A., Mejean, C.O., Boltyanskiy, R., Dufresne, E.R., Angenent, S.B., Altschuler, S.J., Wu, L.F., and Weiner, O.D. (2012). Membrane tension maintains cell polarity by confining signals to the leading edge during neutrophil migration. Cell *148*, 175-188.

Lim, J., and Danuser, G. (2009). Live cell imaging of F-actin dynamics via Fluorescent Speckle Microscopy (FSM). J. Vis. Exp.

Machacek, M., and Danuser, G. (2006). Morphodynamic profiling of protrusion phenotypes. Biophys. J. *90*, 1439-1452.

Machacek, M., Hodgson, L., Welch, C., Elliott, H., Pertz, O., Nalbant, P., Abell, A., Johnson, G.L., Hahn, K.M., and Danuser, G. (2009). Coordination of Rho GTPase activities during cell protrusion. Nature *461*, 99-103.

Mendoza, M.C., Besson, S., and Danuser, G. (2012). Quantitative Fluorescent Speckle Microscopy (QFSM) to Measure Actin Dynamics. Curr. Protoc. Cytom. *Chapter 2*, Unit2 18.

Otsu, N. (1979). A threshold selection method from gray-level histograms. IEEE Trans. Sys., Man, Cyber *9*, 62.

Raucher, D., and Sheetz, M.P. (2000). Cell spreading and lamellipodial extension rate is regulated by membrane tension. J. Cell Biol. *148*, 127-136.

Rizvi, S.A., Neidt, E.M., Cui, J., Feiger, Z., Skau, C.T., Gardel, M.L., Kozmin, S.A., and Kovar, D.R. (2009). Identification and characterization of a small molecule inhibitor of formin-mediated actin assembly. Chem. Biol. *16*, 1158-1168.

Rosin, P. (2001). Uni-modal thresholding. Pattern Recognition *34*, 2083.

Sedzinski, J., Biro, M., Oswald, A., Tinevez, J.Y., Salbreux, G., and Paluch, E. (2011). Polar actomyosin contractility destabilizes the position of the cytokinetic furrow. Nature *476*, 462-466.